

Interpretable ECG Analysis for Myocardial Infarction Detection through Counterfactuals

Toygar Tanyel^a, Sezgin Atmaca^b, Kaan Gökçe^b, M. Yiğit Balık^c, Arda Güler^b, Emre Aslanger^d, İlkay Öksüz^{e,*}

^aBiomedical Engineering Graduate Program, Istanbul Technical University, Istanbul, Türkiye

^bMehmet Akif Ersoy Thoracic and Cardiovascular Surgery Training and Research Hospital, Istanbul, Türkiye

^cDepartment of Computer Science, Aalto University, Espoo, Finland

^dDepartment of Cardiology, Başakşehir Pine and Sakura City Hospital, Istanbul, Türkiye

^eDepartment of Computer Engineering, Istanbul Technical University, Istanbul, Türkiye

Abstract

In the evolving landscape of ECG signal analysis, the opaque nature of deep learning models poses challenges to their integration into clinical practice. This study aims to address these challenges by investigating the application of counterfactual explanations to make machine learning models more interpretable for clinicians, particularly in the context of differentiating control group subjects from myocardial infarction patients. Utilizing the PTB-XL dataset, we developed a methodology for systematic feature extraction and refinement to prepare for counterfactual analysis. This led to the creation of the Visualizing Counterfactual Clues on Electrocardiograms (VCCE) method, designed to improve the practicality of counterfactual explanations in a clinical setting. The validity of our approach was assessed using custom metrics that reflect the diagnostic relevance of counterfactuals, evaluated with the help of two cardiologists. Our findings suggest that this approach could support future efforts in using ECGs to predict patient outcomes for cardiac conditions, achieving interpretation validity scores of 23.29 ± 1.04 and 20.28 ± 0.99 out of 25 for high and moderate-quality interpretations, respectively. Clinical alignment scores of 0.83 ± 0.12 for high-quality and 0.57 ± 0.10 for moderate-quality interpretations underscore the potential clinical applicability of our method. The methodology and findings of this study contribute to the ongoing discussion on enhancing the interpretability of machine learning models in cardiology, offering a concept that bridges the gap between advanced data analysis techniques and clinical decision-making. The source code for this study is available at <https://github.com/tanyelai/vcce>.

Keywords: electrocardiogram, counterfactual explanations, machine learning, myocardial infarction

1. Introduction

Diagnosing myocardial infarction (MI) using electrocardiograms (ECG) remains challenging due to sometimes subtle changes in the ST segment, T wave, and QRS complex [1, 2]. When these changes are not evident, other tests are required for diagnosis. Early research on ECG-based diagnosis focused on machine learning (ML) with handcrafted features or Electronic Health Record (EHR) data [3, 4, 5, 6, 7], utilizing explanation methods like LIME and SHAP to interpret model decisions [8, 9, 10, 11]. However, these methods may not fully meet clinicians' needs for practical, decision-supporting

insights. Recent advancements have shifted towards deep learning, leveraging the entire 12-lead ECG signal for enhanced diagnostic accuracy [12, 13, 14, 15, 16]. Techniques like Grad-CAM have been employed to visually explain predictions [17, 18, 19, 20], though challenges in accurately pinpointing diagnostic signal regions remain.

In healthcare, cognitive biases and counterfactual thinking significantly influence medical decisions [21, 22, 23, 24]. Recent studies have explored statistical alternatives to instinct-based decisions [25, 26], proposing personalized treatments through counterfactual evaluations [27, 28, 29, 30, 31, 32, 33].

Our study introduces a novel approach, utilizing synchronous heartbeat data across all ECG leads to develop a comprehensive feature set. This methodology, Visualizing Counterfactual Clues on Electrocardiograms (VCCE), aims to enhance disease detection and signal

*Corresponding Author. *Addressline:* Istanbul Technical University, ITU Ayazaga Kampusu, Bilgisayar-Bilim Fakültesi, Maslak, 34467 Sarıyer/Istanbul, *Fax:* 0212 285 34 24, *Tel:* 90-212-285-3593

Email address: oksuzilkay@itu.edu.tr (İlkay Öksüz)

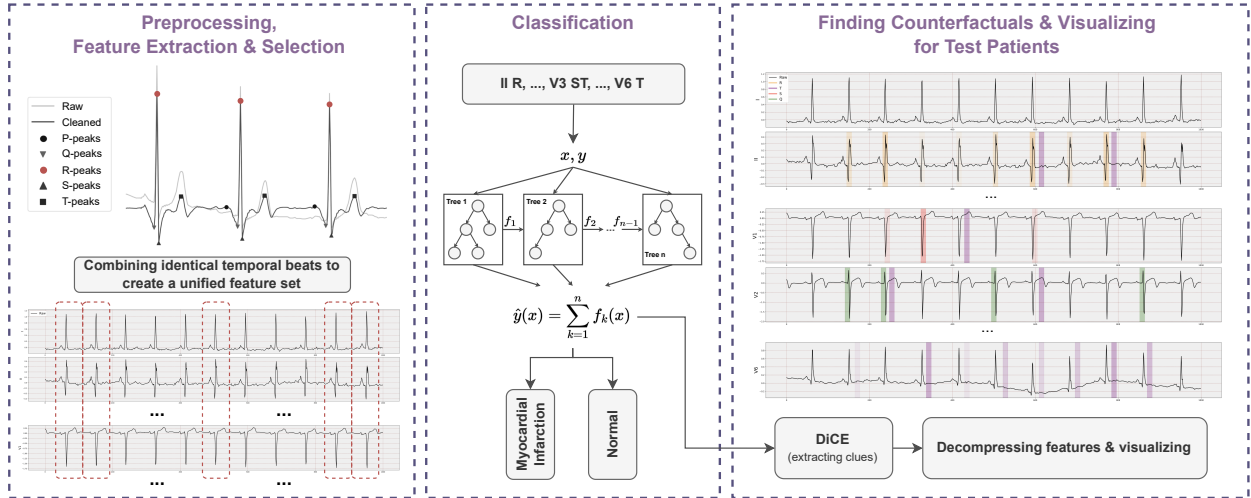


Figure 1: Our proposed pipeline for interpretable ECG classification with improved visualization of counterfactuals has three steps: **1)** Signal preprocessing, extraction and compression of each cardiac cycle, was performed to create a feature set. **2)** The feature set, obtained through a data-driven and domain expertise, was employed to train the XGBoost model for classification. **3)** Counterfactual clues for individual patients were determined using the DiCE method, and the pertinent features were then decompressed and visualized on the ECG reports.

characteristic understanding across leads, providing personalized MI insights and counterfactual visualizations for clearer decision-making support (Figure 1).

We have three major contributions of this work:

- Streamlining feature extraction, ranking, and pruning, enriched with counterfactual insights for a deeper understanding of ECG signals.
- Offering a novel visualization of counterfactual interpretations for 12-lead ECG, facilitating practical application.
- Validating our methods and findings with evaluations from two cardiologists, demonstrating their clinical relevance.

2. Previous Work on Counterfactuals

Exploring human-centric explanations, counterfactuals consider hypothetical "what if" scenarios, offering insights across diverse domains, including philosophy, psychology, and AI [38, 39]. This concept is particularly relevant in medicine, where understanding alternate outcomes could guide patient-specific decisions. AI research has progressively focused on counterfactual generation to personalize responses based on historical cases, thereby enhancing the explanatory depth of ML models [40, 41, 42]. Guidotti’s review [43] and Verma

et al.’s survey [44] offer comprehensive overviews of counterfactual algorithms in ML, with growing interest in their application within ECG analysis [28, 37, 32]. The DiCE algorithm, known for its user-friendliness, has been adopted for generating diverse counterfactual explanations [41].

Counterfactual reasoning extends to fields like finance, medicine, and decision-making, highlighting the versatility of this approach in evaluating future possibilities for individuals [27, 45, 46, 47, 48, 49]. Initial conceptual trade-offs involve the practicality of altering immutable characteristics, such as gender or age, for generating realistic scenarios. Nonetheless, recent algorithms have improved in creating plausible counterfactuals without resorting to unrealistic changes, also allowing the examination of potential biases related to gender, race, or age [50].

3. Dataset

Our study employed the PTB-XL dataset [51] (Version: 1.0.3) at a 100 Hz sampling rate, as increasing it to 500 did not provide significant benefits. We balanced the dataset by randomly undersampling to match the number of normal (NORM) and MI cases, excluding patients with the ST-T changes (STTC) label. The training set comprised 1,559 NORM and 1,559 MI subjects, totaling 14,720 NORM beats and 16,356 MI beats. The test

Paper	Year	Dataset	Sample	Task	Method	Level	ECG Analysis	Clinical Validation	Available Code
Delaney et al. [28]	2021	ECG200	200	Time-series Perturbation	Native Guide	Beat	✗	✗	✓
Looveren et al. [34]	2021	[35]	5000	Time-series Perturbation	Conditional Generative Models	Beat	✗	✗	✗
Wang et al. [36]	2021	TwoLeadECG	1162	Time-series Perturbation	LatentCF++	Beat	✗	✗	✓
Li et al. [37]	2022	ECG200	200	Time-series Perturbation	Motif-Guided	Beat	✗	✗	✗
Todo et al. [32]	2023	PTB-XL	21799	Time-series Perturbation	Contrastive VAE	12-Lead	✗	✗	✗
Nagesh et al. [31]	2023	MIMIC-III	53423	Feature Perturbation	Counterfactual VAE	EHR	✗	✗	✓
Ours	-	PTB-XL	3898	Feature Perturbation	VCCE (Visualization)	12-Lead	✓	✓	✓

Table 1: Comparative overview of counterfactual analysis studies applied to ECG data. This table reviews various studies, all applying methods to ECG data, yet none deeply focus on ECG signals at a clinical level and lack clinical validation. The sample sizes vary, reflecting differences in dataset scales. Some datasets, like ECG200 and TwoLeadECG, are both small in size and scope, focusing on beat-level data. Looveren et al. extract only the first beat from each sample in Baim et al.’s dataset [35]. The PTB-XL dataset, utilized in both Todo et al.’s study and ours, is notably complex than other datasets. Time-series perturbation refers to alterations in the signal itself, whereas feature perturbation involves changes to features extracted from the signal or data sources like electronic health records (EHR). VAE (Variational Autoencoder).

set included 390 subjects from each group, with 3,704 NORM beats and 4,134 MI beats. We excluded patients with subendocardial injury and posterior MI (PMI) due to diagnostic accuracy concerns and prioritized localized MI labels in cases of overlap, ensuring all included cases had 100% certainty levels. The dataset was split 80% for training and 20% for testing, extracting 194 beat-level features across all 12 leads without considering age and gender to prevent bias. For clinical validation of visualized counterfactual clues, 51 random patients were analyzed.

4. Methods

4.1. Preprocessing

For the preprocessing of the raw ECG signals, we primarily utilized the NeuroKit2 library [52] (version 0.2.5) in Python (version 3.9.13). Both denoising and peak detection were accomplished using the method described in [53] (see Supplementary Figures C.1-C.4).

We excluded the initial and final beats to ensure the consistency of the utilized beat signals. Specifically, we omitted these beats to ensure the extraction of RR_prev and RR_next features (Table 2), which necessitate calculations before or after the R peak. While we could have

assigned NaN or 0 values to these features, opting to remove the corresponding beats is advantageous, because this approach mitigates opening and closing errors for the overall signal, hence also contributes to improved signal quality.

4.2. Feature Extraction

In our feature extraction framework, we identified features that might be relevant for uncovering clues. In our framework, we focused on two types of features: temporal and amplitude. Temporal attributes, consistent across all leads, contribute to a more uniform analysis when dealing with ECG tasks, even though they are not the central focus of our framework. Alongside these, we analyzed amplitude variations for each lead. The integration of both temporal and amplitude features resulted in a comprehensive feature set, amounting to a total of 194 features. This blend of temporal and amplitude aspects offers a thorough approach to our analysis. The temporal features, being time-dependent, exhibit a uniform pattern across different leads, whereas the amplitude features vary for each lead and possess distinct properties. These extracted features are comprehensively described in Table 2.

All Leads Common (Time Dependent)		For Each Lead (Time Independent)	
RR_Prev	Previous RR interval	R	R amplitude
RR_Next	Subsequent RR interval	P	P amplitude
RR_Rate	RR_Next / RR_Prev	Q	Q amplitude
PR_int	Time between P_onset and R_onset	S	S amplitude
PR_seg	Time between P_offset and R_onset	T	T amplitude
QRS	Time between R_onset and R_offset	PQ	P_a - Q_a
P_Wave	Time between P_onset and P_offset	QR	Q_a - R_a
T_Wave	Time between T_onset and T_offset	RS	R_a - S_a
T_left	Time between T_onset and T_peak	ST	S_a - T_a
QT	Time between R_onset and T_offset	PS	P_a - S_a
QTc	Corrected QT according to Bazett's formula	PT	P_a - T_a
ST	Time between R_offset and T_onset	QS	Q_a - S_a
PT	Time between P_onset and T_offset	QT	Q_a - T_a
PS	Time between P_onset and S_offset	ST_mean	Mean(ST segment values)
		ST_std	STD(ST segment values)

Table 2: Extracted features. The left-hand side shows the temporal (time-dependent) features, while the right side shows the non-temporal (time-independent) features. The abbreviation 'Waveform_a' denotes the amplitude of a waveform.

4.3. Feature Selection

To enhance ML model training and counterfactual scenario relevance by avoiding feature overload, we streamlined feature selection using recursive feature elimination (RFE) with the XGBoost (XGB) algorithm, isolating 97 top-ranked features focused on engineering. These features were re-evaluated within the XGB framework to refine their importance (Supplementary Figure C.5a). We adopted a methodical training approach, progressively incorporating features from one to the complete 97, recording performance at each increment (Supplementary Figure C.5b).

For counterfactual generation, we selected feature sets in increments of 5 up to 20, noting this process is a post-model development step. The final feature set was enhanced by blending domain knowledge with data-driven insights, particularly through the addition of four key features to the top 20, aimed at boosting diagnostic precision for specific cases (Table 3).

4.4. Counterfactual Generation Process

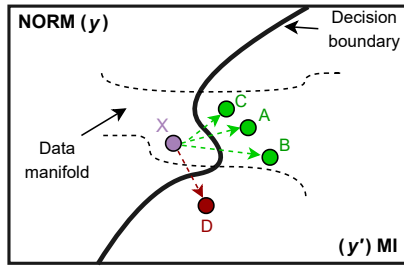
Our counterfactual generation process (Figure 2) integrates the DiCE ML library [41] with a machine learning classifier, specifically an XGBoost model, to produce explainable AI outcomes. The process involves several key steps: classifier training, initialization of DiCE explainer, counterfactual generation, exploration, and data transformation for analysis.

4.5. VCCE: Visualizing Counterfactual Clues on Electrocardiograms

We have developed VCCE (Algorithm 1), a method to enhance the presentation of counterfactual clues in ECG reports for clinicians. This method integrates counterfactual data with extracted ECG features, emphasizing significant waveform features (PQRST) and highlighting their diagnostic implications. VCCE employs a dynamic visualization approach, adapting to various counterfactual scenarios and their impacts on ECG waveforms.

For visualization, VCCE offers options to display peaks (such as the R peak) and chosen amplitude features (like II_R), as identified by the counterfactual algorithm, in selected regions. Advanced features (for example, V3_ST), which are calculated based on amplitude differences between two peaks, are represented as lines with their distance values overlaid on the ECG signal (refer to Supplementary Figure C.7). Additionally, in the visualization of counterfactuals, the frequency with which a particular amplitude feature is chosen in an alternative scenario directly influences its prominence in the ECG report. The more often a feature is selected, the more distinctly it is highlighted.

This approach, adaptable beyond the specific ECG task, allows us to observe changes in the PQRST complex across multiple "possible worlds," offering a way to perceive alterations across various scenarios. The primary rationale for assuming the applicability of a



Features	X	A	B	C	D
II_R	0.5155	-0.1178	-1.0497	-	-
II_T	-0.0126	-	-	-0.7824	-
V4_R	1.2262	-	-	-	-
V3_R	0.9451	-	-	-	-
aVF_R	0.1803	-0.4741	-	-	-0.3021
*Gender	M	-	-	-	F

*Gender is used metaphorically only to represent the 'D' condition, the remaining features have real values.

Figure 2: The illustration of generating counterfactual explanations for NORM to MI case. The figure on the left depicts details of what happens during this process and the concept of "counterfactual generation". On the right side, the illustration provides an example of the generated cases involved in the process (X to A, B, C or D). The green is for valid counterfactuals, while the red is representing fanciful generations. The symbol "-" signifies that the feature remained unchanged. Key ECG signal features are labeled: II_R (R amplitude of lead II), II_T (T amplitude of lead II), V4_R (R amplitude of lead V4), V3_R (R amplitude of lead V3), and aVF_R (R amplitude of lead aVF). M: Male, F: Female. Data manifold represents real-life constraints, such as Gender.

Algorithm 1 VCCE Pseudocode

```

1: procedure VCCE(signal, extracted_features, counterfactuals, feature_count)
2:   feature_list  $\leftarrow$  [P, Q, R, S, T, ST, PT, RS, QS]
3:   lead_names  $\leftarrow$  [I, II, III, aVR, aVL, aVF, V1, V2, V3, V4, V5, V6]
4:   combined_data  $\leftarrow$  PREPAREDATA(counterfactuals, extracted_features)
5:   visualization_df  $\leftarrow$  CREATEVISUALIZATIONGRAPH(combined_data, feature_count)
6:   for each lead in lead_names do
7:     for each feature in feature_list do
8:       peaks  $\leftarrow$  EXTRACTPEAKS(visualization_df, lead, feature)
9:       PLOTPEAKS(peaks, signal, lead)
10:      PLOTDOTTEDLINES(peaks, signal, lead)
11:      PLOTEMPHASIS(peaks, signal, lead)
12:    end for
13:  end for
14:  PLOTECGREPORT(signal, visualization_df, ...)
15: end procedure

```

► For advanced features

VCCE-like approach across a range of ECG tasks lies in the nature of the ECG features employed, which are similar to those used in other ECG-dependent cardiac conditions. These features are extracted based on the structure of the P-, Q-, R-, S-, and T-waveforms (cardiac cycle) at the beat level, a consistent factor across all ECGs. The key advantage is that these derived features provide distinct temporal and amplitude-level information that is inherently interpretable. As a result, we can not only numerically analyze the generated counterfactual scenarios but also visually assess their impact on specific waves within particular leads and beats.

In the proposed study, we note that the selected top

20 features are predominantly time independent due to their dependence on lead-wise amplitude characteristics across all MI cases in the dataset, with RR_Next being the only temporal one. Therefore, our visualization method primarily focuses on amplitude-based (non-temporal) features. Additionally, we have included four more features (V2_T, V3_T, V4_T, and V6_T), selected by domain experts, to enhance individual resolution, such as distinguishing between inferior and anterior case differences. Consequently, we initiate a decoding process to unfold the temporally compressed beats. This decoding involves expanding the feature names to indicate the specific area influenced by the counterfactuals

responsible for the change, encompassing details such as the lead, the waveform feature, and the beat associated with the counterfactual’s impact. This way, we are individually marking the features that contribute the most significant distinction between the two diagnoses.

4.6. Evaluation Metrics

We utilize common metrics in ML (precision, recall, and F1 score), and present a set of custom evaluation metrics used to assess the plausibility of the generated counterfactual clues for ECG signals. The metrics are designed to capture both the clinical relevance of the counterfactual changes and the simplicity of the explanations. For detailed explanation of the metrics, see Supplementary Section A.

5. Experimental Results

5.1. Model Selection

We opted for the XGBoost model in this study because it maintains a balance across all metrics and offers the highest scores (refer to Supplementary Section B).

5.2. Feature Elimination and XGBoost Classification

For the training of the ML model, our initial step involved employing RFE on XGB to reduce the number of features. This process assigned a rank of 1 to 97 features, and we proceeded with our analysis using this subset of selected features. In subsequent stages of our analysis, we computed the importances of these chosen features within the XGB, as depicted in Supplementary Figure C.5.

Following an in-depth examination of the selected features, we organized them based on their respective importance scores. Then, we conducted further training on XGB, progressively augmenting the number of features employed in the model (Supplementary Figure C.5b), where we can observe that having a mere 2% score tolerance enables us to reduce the feature count from 86 to 19. This reduction brings benefits when working with counterfactuals.

Through our experimental investigations, we discovered that utilizing 19 features is sufficient for extracting counterfactual instances. A lesser number of features is preferable for counterfactuals as it yields better and more reasonable explanations. To conduct a comprehensive assessment of counterfactuals, we generated distinct scenarios involving sets of 5, 10, 15, and 20 features. This evaluation encompassed considerations such as the time taken for generation (refer to Supplementary Figure C.6) and a comparative analysis of the most influential

features affecting the outcomes. The F1 scores for each feature set are as follows: 81.40% for 5 features, 83.50% for 10 features, 85.83% for 15 features, 86.59% for 20 features, and 88.47% for 97 features.

R-wave amplitude stands out as a prominent feature in the initial set of features (4 out of 5). We also observe the importance of T-wave amplitude in lead II and aVR, as well as S-wave amplitude in lead V1. Additionally, we notice T-waves with a lesser impact in V1 and V5 leads. In the case of V3 and V1, we observe various peak relationships, specifically the differences between S-amplitude and T-amplitude at V3, R-amplitude and S-amplitude, P-amplitude and S-amplitude, Q-amplitude and S-amplitude, as well as S-amplitude and T-amplitude at V1.

5.3. Counterfactual Instance Generation

To generate counterfactual instances, we proceeded with the chosen feature sets of 5, 10, 15, and 20 during the Section 5.2. Table 4 provides a comprehensive overview of the outcomes, illustrating transformations from MI patients to NORM and vice versa. Specifically, a feature that is altered more frequently across different cases is considered more indicative or critical for changing the classification outcome. Thus, in the search for counterfactuals, those features that are most frequently chosen for alteration are highlighted as the most important or influential features in determining the class of a heartbeat. This insight is crucial for understanding which aspects of the data are most pivotal in the ML model’s decision-making process and can guide efforts to improve model accuracy and interpretability.

In the counterfactual analysis conducted across a population of beats, it becomes evident that the XGB model more easily diagnoses beats from NORM patients compared to those from MI patients. This observation is supported by the pred/true ratio, which is detailed in Table 4. Among the features under consideration, Feature 1-3 correspond to the top three features selected through the counterfactual optimization process. This selection indicates that these specific features exhibit better differentiation between NORM and MI cases, with distinct value distributions when we compare instances labeled as NORM to those categorized as MI. Consequently, we provided the most significant features by conducting additional feature selection across "possible worlds," for the collection of beats.

Analyzing the transition from NORM to MI, we observed notable changes in aVF_R, V3_ST, and II_R among different feature sets. For the inverse transition, from MI to NORM, the features II_T and II_R underwent substantial changes.

Top 20 Features				4 Features Included by Clinicians	
1) II_R: 24	6) V1_S: 15	11) V1_PS: 0	16) V4_PT: 2	21) V2_T: 24	
2) II_T: 24	7) aVR_T: 5	12) aVF_QS: 0	17) V2_Q: 17	22) V3_T: 24	
3) V4_R: 18	8) V3_ST: 22	13) V1_QS: 0	18) V1_T: 5	23) V4_T: 18	
4) V3_R: 16	9) aVF_ST_mean: 23	14) V1_ST: 19	19) V5_T: 20	24) V6_T: 19	
5) aVF_R: 15	10) V1_RS: 6	15) RR_Next: 4	20) aVL_RS: 13		

Table 3: Top 20 features after our selection process, along with an additional 4 features chosen by clinicians. Moreover, we present the general clinical importance scores assigned by domain experts for each selected feature out of 24 points.

	NORM to MI				MI to NORM			
	5 features	10 features	15 features	20 features	5 features	10 features	15 features	20 features
Pred/True	50/50	48/50	50/50	49/50	45/50	45/50	45/50	46/50
1st Significant	aVF_R: 60	V3_ST: 54	II_R: 37	V3_ST: 43	II_T: 66	II_T: 56	II_R: 60	II_R: 71
2nd Significant	II_R: 56	V1_S: 36	V3_ST: 37	V2_Q: 34	aVF_R: 43	aVF_R: 50	II_T: 39	V3_R: 59
3rd Significant	II_T: 45	II_T: 35	II_T: 35	II_R: 31	II_R: 42	II_R: 37	aVF_R: 38	V4_PT: 36

Table 4: The table displays the key altered features across four distinct feature sets, accompanied by counterfactual cases from a sample of 50 heartbeats. In this context, an 'altered feature' is defined as a feature whose modification significantly influences the predicted class of a heartbeat in the ML model. The frequency at which a feature is altered in these counterfactual scenarios reflects its relative importance. 'Pred' represents the label assigned by the ML model, and 'True' indicates the actual class label of the heartbeats. This analysis focuses on heartbeats that the ML model accurately classified, excluding any counterfactuals from misdiagnosed cases. For each heartbeat, three counterfactual explanations are generated. For instance, if the feature set shows a pred/true ratio of 45/50, this leads to a total of 150 counterfactuals. However, considering 5 misdiagnoses, only 135 counterfactuals are used for statistical analysis. As an example, in the transition from MI to NORM, the II_T feature changes 66 times within 135 possible scenarios for the selected 5 features set.

Generation times for counterfactual instances varied with the feature count. For NORM to MI transitions, generation times were 17.71 ± 33.0 seconds (5 features), 35.35 ± 45.62 seconds (10 features), 46.86 ± 53.35 seconds (15 features), and 58.06 ± 61.8 seconds (20 features). For MI to NORM transitions, generation times were notably higher: 73.2 ± 106.46 seconds (5 features), 132.64 ± 259.36 seconds (10 features), 111.94 ± 121.75 seconds (15 features), and 127.48 ± 129.02 seconds (20 features). This demonstrates that transitions from MI to NORM are more time-consuming and complex, reflecting the greater challenge and optimization effort required for these cases.

5.4. Visualization of Counterfactual Clues

We utilized I-1 to assess the quality of interpretability, I-2 to determine clinical alignment, I-3 to account for individual waveform errors corresponding to the validity score, and I-4 to evaluate clinical sparsity, which is expected to differ from XGBoost's sparsity based on feature importances. For detailed descriptions of the

evaluation metrics I-1, I-2, I-3, and I-4, please refer to the Supplementary Section A.

In addition to the analysis in Section 5.3, our preliminary empirical investigations on visual assessments have led domain experts to conclude that the incorporation of four additional features (V2_T, V3_T, V4_T, and V6_T) can be both beneficial and necessary. These features have not only enhanced the quality of visualization but also improved the classification accuracy. This was evident in the identification of local MI cases, such as Case ID 3234.0 in the dataset, where the system accurately identified 6 out of 7 individual beats, an improvement from the prior accuracy of 2 out of 7.

51 reports were evaluated (Figure 4); 5 of them were excluded due to extreme artifacts ($n=1, \mu=0$) and ventricular extrasystole ($n=4, 10.25 \pm 5.5$). Of the remaining 46 reports, 17 were categorized as high (23.29 ± 1.04), 14 as moderate (20.28 ± 0.99), and 15 as low (11.20 ± 7.76) in terms of interpretability. The " \pm " symbol represents the mean and standard deviation of validation scores, respectively. A total of 31 reports were identified

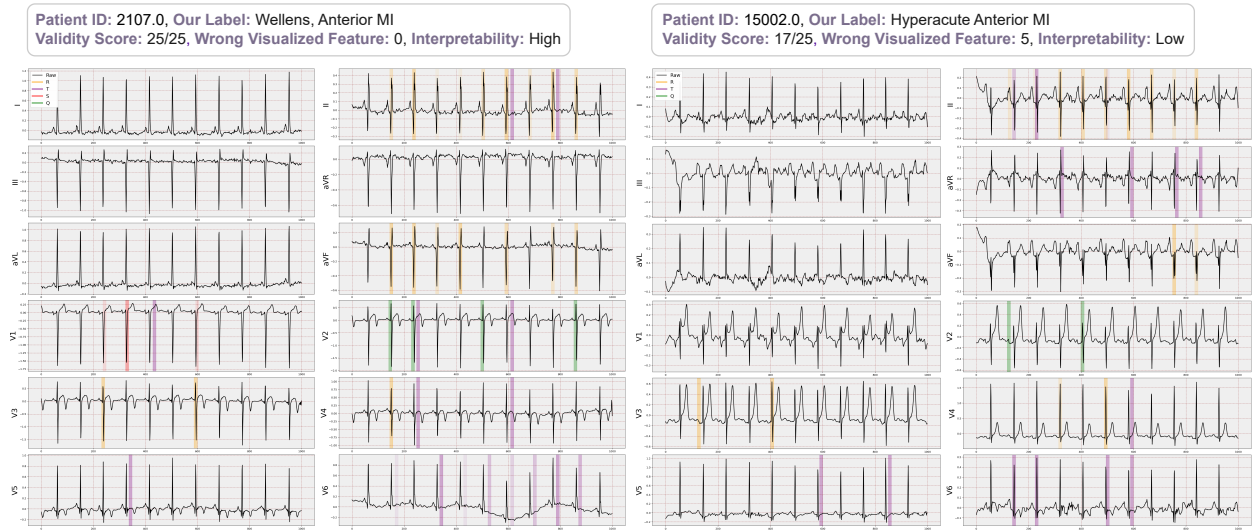


Figure 3: Two example reports with visualized clues. Left: Patient’s report with good and sufficient markings. Right: Patient’s report with some unnecessary or incorrect markings, affecting interpretability scores.

as acceptable.

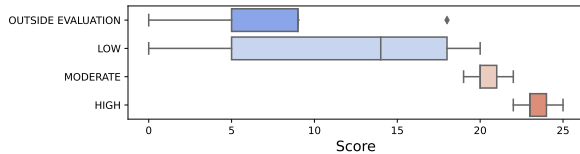


Figure 4: Validation score distribution on interpretability.

In terms of overall counterfactual sparsity, by using our clinical scoring (I-4), counterfactuals demonstrated lower sparsity (0.19) compared to the XGB feature importances as scoring, which had a sparsity of 0.33. Patient-wise differences can be observed by comparing clinical and XGB boxplots. The general sparsity in XGB is evident in the Figure 5, although some cases displayed even lower sparsity than their clinical-weighted counterparts.

In the alignment of blind evaluations and identified clues, we obtained scores of 0.83 ± 0.12 for high-quality reports, 0.57 ± 0.10 for moderate-quality reports, and 0.22 ± 0.24 for low-quality reports. We observed that a many of the low-quality reports were attributed to incorrect peak detection, which inevitably resulted in their low-quality classification. Moreover, these low-quality reports often contained labels that were inconsistent with our blind evaluations and the original labels.

For more detailed clinical explanations of some of the

selected cases, please refer to Figures C.8, C.9, and C.10 in the Supplementary Material.

6. Discussion

AI integration into healthcare faces challenges, notably clinician concerns over AI decision-making. Despite advancements, making AI decisions understandable is difficult. Our study focuses on explainable AI (XAI), specifically counterfactual explanations, to demystify ML decisions in ECG analysis with VCCE.

We chose the XGB algorithm for its superior performance (89.36% AUC) on the PTB-XL dataset after comparing several ML algorithms. The XGB model’s `max_depth` parameter helps avoid overfitting, and we optimized to maintain performance with minimal complexity, selecting 20 features while considering dataset noise and ensuring high model accuracy.

To address potential bias driven by data, we incorporated four features recommended by clinicians to enhance local clues. Counterfactual explanations refine feature selection by adding minimal yet impactful modifications, which improve model performance and provide a more nuanced understanding of the data.

Our model, with 86.3% accuracy using 19 features, faces challenges with ventricular extrasystole (VES) and bundle branch blocks due to their unique morphologies. The reliance on standard evaluation criteria for these conditions can lead to inaccuracies. The PTB-XL dataset’s

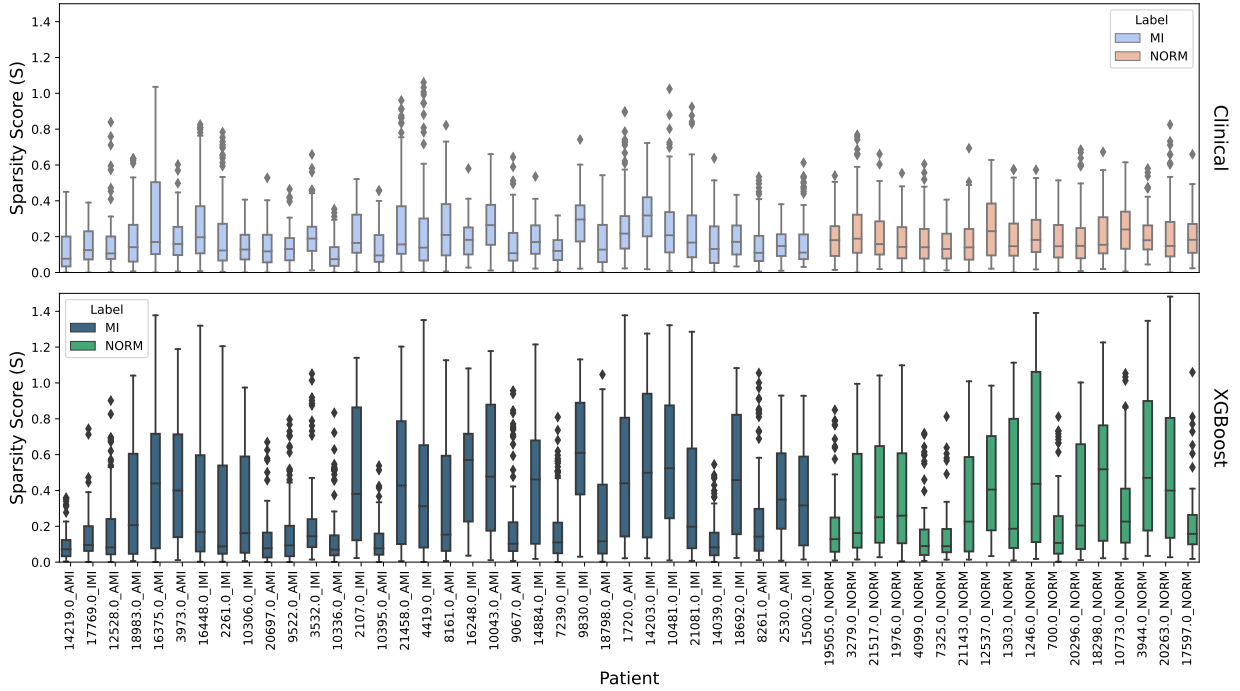


Figure 5: Counterfactual sparsity scores. In this figure, patients with AMI and IMI are definitively diagnosed with Anterior MI and Inferior MI, respectively, according to the original dataset labels. NORM cases serve as the control group. Counterfactuals are weighted by clinical importance score and XGB feature importance, and we compared their sparsity scores. A higher sparsity score indicates a greater divergence from the original sample. This is because important features are selected more often, resulting in a more diverse counterfactual sample. The box plot represents all beats for patients and the corresponding counterfactual for each beat.

label reliability is also questioned. While most studies accept the labels as they are [54, 55], our blind evaluations identified numerous undecidable cases from ECG readings, and there were potentially wrongly interpreted patients.

Blind evaluations of counterfactual explanations showed they provide meaningful insights without contradictions, supported by expert annotations. Our method’s use of sparsity and cognitive interpretability scores (17 high, 14 moderate, 15 low) alongside validity scores (0.83 for high, 0.57 for moderate, and 0.22 for low) demonstrates the effectiveness and promise of counterfactual explanations in enhancing understanding of ML decisions in ECG analysis.

In counterfactual research, including ECG analysis, diverse algorithms have been developed, focusing on signal perturbation within short, restricted beats [28, 36, 37]. Our approach uniquely analyzes entire 10-second beats from 12-lead ECGs collectively, offering comprehensive insights into the entire ECG report. Despite generative

methods’ potential, existing research [34, 32] often lacks clinical grounding and open-source code, with some studies [31] not prioritizing ECG analysis. This reflects a broader issue: current studies fail to align with clinical needs, using metrics like sparsity and validity that hold limited medical relevance due to the lack of suitable datasets for their application. Addressing this gap, our work introduces new metrics designed for medical contexts and demonstrates the clinical importance of analyzing 12-lead counterfactuals. However, communicating these findings to clinicians effectively remains challenging with existing methods. Our innovative approach, validated by cardiologists, presents a promising direction for future research, illustrating the potential to bridge the gap between counterfactual research and practical clinical application.

This study has several limitations that offer directions for future research. The accuracy of results may be impacted by the variability in peak detection performance on amplitude values, addressed partially by employing

the [53] method. However, high-noise and irregular heart rhythm scenarios remain challenging. The absence of visible active heart rhythm waves in some beats due to external factors during ECG recordings could lead to inaccurately indexed beats; this was mitigated by excluding such beats during visualization. Additionally, the study did not assess the entire signal in one go but analyzed all leads for each heartbeat to determine patient outcomes. Lastly, the optimization duration of the DiCE method during counterfactual generation poses a limitation, but exploring alternative algorithms may offer solutions. These limitations provide a foundation for enhancing visualization methods and exploring diverse features in future works.

7. Conclusion

Our study proposes a novel idea for improving ECG analysis by integrating counterfactual explanations with our VCCE visualization technique. By merging AI insights with expert cardiologist evaluations, we offer a perspective on MI analysis. Our approach, validated through custom metrics and comprehensive evaluations, shows potential for enhanced visualization and diagnostic precision. This research provides a stepping stone for future work aimed at refining AI applications and addressing cognitive needs in medical contexts.

Funding

This study was supported by the TUSEB 2022-EKG-01 Program (Project No: 20101).

References

- [1] A. A. Panju, B. R. Hemmelgarn, G. H. Guyatt, D. L. Simel, Is this patient having a myocardial infarction?, *Jama* 280 (1998) 1256–1263.
- [2] K. Thygesen, J. S. Alpert, H. D. White, Universal definition of myocardial infarction, *circulation* 116 (2007) 2634–2653.
- [3] W. Dai, T. S. Brisimi, W. G. Adams, T. Mela, V. Saligrama, I. C. Paschalidis, Prediction of hospitalization due to heart diseases by supervised learning methods, *International journal of medical informatics* 84 (2015) 189–197.
- [4] L. D. Sharma, R. K. Sunkaria, Inferior myocardial infarction detection using stationary wavelet transform and machine learning approach, *Signal, Image and Video Processing* 12 (2018) 199–206.
- [5] R. Alizadehsani, M. Abdar, M. Roshanzamir, A. Khosravi, P. M. Kebria, F. Khozimeh, S. Nahavandi, N. Sarrafzadegan, U. R. Acharya, Machine learning-based coronary artery disease diagnosis: A comprehensive review, *Computers in biology and medicine* 111 (2019) 103346.
- [6] N. Ibtehaz, M. S. Rahman, M. S. Rahman, Vfpred: a fusion of signal processing and machine learning techniques in detecting ventricular fibrillation from ecg signals, *Biomedical Signal Processing and Control* 49 (2019) 349–359.
- [7] Y. M. Ayano, F. Schwenker, B. D. Dufera, T. G. Debelee, Interpretable machine learning techniques in ecg-based heart disease classification: a systematic review, *Diagnostics* 13 (2022) 111.
- [8] M. T. Ribeiro, S. Singh, C. Guestrin, "why should i trust you?": Explaining the predictions of any classifier, in: *Proceedings of the 22nd ACM SIGKDD International Conference on Knowledge Discovery and Data Mining, KDD '16*, Association for Computing Machinery, New York, NY, USA, 2016, p. 1135–1144. URL: <https://doi.org/10.1145/2939672.2939778>. doi:10.1145/2939672.2939778.
- [9] S. Lundberg, S.-I. Lee, A unified approach to interpreting model predictions, 2017. [arXiv:1705.07874](https://arxiv.org/abs/1705.07874).
- [10] M. Bodini, M. W. Rivolta, R. Sassi, Interpretability analysis of machine learning algorithms in the detection of st-elevation myocardial infarction, in: *2020 Computing in Cardiology, IEEE, 2020*, pp. 1–4.
- [11] M. K. Shetty, S. Kunal, M. Girish, A. Qamar, S. Arora, M. Hendrickson, P. P. Mohanan, P. Gupta, S. Ramakrishnan, R. Yadav, et al., Machine learning based model for risk prediction after st-elevation myocardial infarction: Insights from the north india st elevation myocardial infarction (norin-stemi) registry, *International Journal of Cardiology* 362 (2022) 6–13.
- [12] S. Hong, Y. Zhou, J. Shang, C. Xiao, J. Sun, Opportunities and challenges of deep learning methods for electrocardiogram data: A systematic review, *Computers in biology and medicine* 122 (2020) 103801.
- [13] N. I. Hasan, A. Bhattacharjee, Deep learning approach to cardiovascular disease classification employing modified ecg signal from empirical mode decomposition, *Biomedical signal processing and control* 52 (2019) 128–140.
- [14] G. Paragliola, A. Coronato, An hybrid ecg-based deep network for the early identification of high-risk to major cardiovascular events for hypertension patients, *Journal of Biomedical Informatics* 113 (2021) 103648.
- [15] A. Gupta, E. Huerta, Z. Zhao, I. Moussa, Deep learning for cardiologist-level myocardial infarction detection in electrocardiograms, in: *8th European Medical and Biological Engineering Conference: Proceedings of the EMBEC 2020, November 29–December 3, 2020 Portorož, Slovenia, Springer, 2021*, pp. 341–355.
- [16] L. Wu, G. Huang, X. Yu, M. Ye, L. Liu, Y. Ling, X. Liu, D. Liu, B. Zhou, Y. Liu, et al., Deep learning networks accurately detect st-segment elevation myocardial infarction and culprit vessel, *Frontiers in cardiovascular medicine* 9 (2022) 797207.
- [17] M. Y. Balık, K. Gökçe, S. Atmaca, E. Aslanger, A. Güler, İ. Öksüz, Interpretable deep learning for myocardial infarction detection from ecg signals, in: *2023 31st Signal Processing and Communications Applications Conference (SIU), IEEE, 2023*, pp. 1–4.
- [18] H. Makimoto, M. Höckmann, T. Lin, D. Glöckner, S. Gerguri, L. Clasen, J. Schmidt, A. Assadi-Schmidt, A. Bejinariu, P. Müller, et al., Performance of a convolutional neural network derived from an ecg database in recognizing myocardial infarction, *Scientific reports* 10 (2020) 8445.
- [19] V. Jahmunah, E. Y. K. Ng, R.-S. Tan, S. L. Oh, U. R. Acharya, Explainable detection of myocardial infarction using deep learning models with grad-cam technique on ecg signals, *Computers in Biology and Medicine* 146 (2022) 105550.
- [20] R. R. Selvaraju, M. Cogswell, A. Das, R. Vedantam, D. Parikh, D. Batra, Grad-cam: Visual explanations from deep networks via gradient-based localization, in: *Proceedings of the IEEE*

- international conference on computer vision, 2017, pp. 618–626.
- [21] J. Chen, Z. Gandomkar, W. M. Reed, Investigating the impact of cognitive biases in radiologists’ image interpretation: A scoping review, *European Journal of Radiology* (2023) 111013.
- [22] J. V. Petrocelli, Pitfalls of counterfactual thinking in medical practice: Preventing errors by using more functional reference points, *Journal of Public Health Research* 2 (2013) jphr–2013.
- [23] J. E. Groopman, M. Prichard, *How doctors think*, volume 82, Houghton Mifflin Boston, 2007.
- [24] R. Durand, E. Vaara, Causation, counterfactuals, and competitive advantage, *Strategic Management Journal* 30 (2009) 1245–1264.
- [25] G. Gigerenzer, W. Gaissmaier, E. Kurz-Milcke, L. M. Schwartz, S. Woloshin, Helping doctors and patients make sense of health statistics, *Psychological science in the public interest* 8 (2007) 53–96.
- [26] R. H. Riffenburgh, D. L. Gillen, *Statistics in medicine*, Academic press, 2020.
- [27] Z. Wang, I. Samsten, P. Papapetrou, Counterfactual explanations for survival prediction of cardiovascular icu patients, in: *Artificial Intelligence in Medicine: 19th International Conference on Artificial Intelligence in Medicine, AIME 2021, Virtual Event, June 15–18, 2021, Proceedings*, Springer, 2021, pp. 338–348.
- [28] E. Delaney, D. Greene, M. T. Keane, Instance-based counterfactual explanations for time series classification, in: *International Conference on Case-Based Reasoning*, Springer, 2021, pp. 32–47.
- [29] S. Haldar, P. G. John, D. Saha, Reliable counterfactual explanations for autoencoder based anomalies, in: *Proceedings of the 3rd ACM India Joint International Conference on Data Science & Management of Data (8th ACM IKDD CODS & 26th COMAD)*, 2021, pp. 83–91.
- [30] R. Xu, Y. Yu, C. Zhang, M. K. Ali, J. C. Ho, C. Yang, Counterfactual and factual reasoning over hypergraphs for interpretable clinical predictions on ehr, in: *Machine Learning for Health*, PMLR, 2022, pp. 259–278.
- [31] S. Nagesh, N. Mishra, Y. Naamad, J. M. Reh, M. A. Shah, A. Wagner, Explaining a machine learning decision to physicians via counterfactuals, in: *Conference on Health, Inference, and Learning*, PMLR, 2023, pp. 556–577.
- [32] W. Todo, M. Selmani, B. Laurent, J.-M. Loubes, Counterfactual explanation for multivariate times series using a contrastive variational autoencoder, in: *ICASSP 2023-2023 IEEE International Conference on Acoustics, Speech and Signal Processing (ICASSP)*, IEEE, 2023, pp. 1–5.
- [33] T. Tanyel, S. Ayvaz, B. Keserci, Beyond known reality: Exploiting counterfactual explanations for medical research, *arXiv preprint arXiv:2307.02131* (2023).
- [34] A. Van Looveren, J. Klaise, G. Vacanti, O. Cobb, Conditional generative models for counterfactual explanations, *arXiv preprint arXiv:2101.10123* (2021).
- [35] D. S. Baim, W. S. Colucci, E. S. Monrad, H. S. Smith, R. F. Wright, A. Lanoue, D. F. Gauthier, B. J. Ransil, W. Grossman, E. Braunwald, Survival of patients with severe congestive heart failure treated with oral milrinone, *Journal of the American College of Cardiology* 7 (1986) 661–670.
- [36] Z. Wang, I. Samsten, R. Mochaourab, P. Papapetrou, Learning time series counterfactuals via latent space representations, in: *Discovery Science: 24th International Conference, DS 2021, Halifax, NS, Canada, October 11–13, 2021, Proceedings* 24, Springer, 2021, pp. 369–384.
- [37] P. Li, S. F. Boubrahimi, S. M. Hamdi, Motif-guided time series counterfactual explanations, in: *International Conference on Pattern Recognition*, Springer, 2022, pp. 203–215.
- [38] T. Miller, Explanation in artificial intelligence: Insights from the social sciences, *Artificial intelligence* 267 (2019) 1–38.
- [39] W. Starr, Counterfactuals, in: E. N. Zalta, U. Nodelman (Eds.), *The Stanford Encyclopedia of Philosophy*, Winter 2022 ed., Metaphysics Research Lab, Stanford University, 2022.
- [40] S. Wachter, B. Mittelstadt, C. Russell, Counterfactual explanations without opening the black box: Automated decisions and the gdpr, *Harv. JL & Tech.* 31 (2017) 841.
- [41] R. K. Mothilal, A. Sharma, C. Tan, Explaining machine learning classifiers through diverse counterfactual explanations, in: *Proceedings of the 2020 conference on fairness, accountability, and transparency*, 2020, pp. 607–617.
- [42] Y.-L. Chou, C. Moreira, P. Bruza, C. Ouyang, J. Jorge, Counterfactuals and causability in explainable artificial intelligence: Theory, algorithms, and applications, *Information Fusion* 81 (2022) 59–83.
- [43] R. Guidotti, Counterfactual explanations and how to find them: literature review and benchmarking, *Data Mining and Knowledge Discovery* (2022) 1–55.
- [44] S. Verma, V. Boonsanong, M. Hoang, K. E. Hines, J. P. Dickerson, C. Shah, Counterfactual explanations and algorithmic recourses for machine learning: A review, *arXiv preprint arXiv:2010.10596* (2020).
- [45] S. O. Fogel, T. Berry, The disposition effect and individual investor decisions: the roles of regret and counterfactual alternatives, *The journal of behavioral finance* 7 (2006) 107–116.
- [46] L. Yang, E. M. Kenny, T. L. J. Ng, Y. Yang, B. Smyth, R. Dong, Generating plausible counterfactual explanations for deep transformers in financial text classification, *arXiv preprint arXiv:2010.12512* (2020).
- [47] M. Höfler, Causal inference based on counterfactuals, *BMC medical research methodology* 5 (2005) 1–12.
- [48] A. Waters, R. Miikkulainen, Grade: Machine learning support for graduate admissions, *Ai Magazine* 35 (2014) 64–64.
- [49] M. Andini, E. Ciani, G. De Blasio, A. D’Ignazio, V. Salvestrini, Targeting policy-compliers with machine learning: an application to a tax rebate programme in italy, *Bank of Italy Temi di Discussione (Working Paper) No 1158* (2017).
- [50] A. Mikotajczyk, M. Grochowski, A. Kwasięroch, Towards explainable classifiers using the counterfactual approach: global explanations for discovering bias in data, *Journal of Artificial Intelligence and Soft Computing Research* 11 (2021) 51–67.
- [51] P. Wagner, N. Strodthoff, R.-D. Boussejot, D. Kreisler, F. I. Lunze, W. Samek, T. Schaeffter, Ptb-xl, a large publicly available electrocardiography dataset, *Scientific data* 7 (2020) 154.
- [52] D. Makowski, T. Pham, Z. J. Lau, J. C. Brammer, F. Lespinasse, H. Pham, C. Schölzel, S. A. Chen, Neurokit2: A python toolbox for neurophysiological signal processing, *Behavior research methods* (2021) 1–8.
- [53] T. Koka, M. Muma, Fast and sample accurate r-peak detection for noisy ecg using visibility graphs, in: *2022 44th Annual International Conference of the IEEE Engineering in Medicine & Biology Society (EMBC)*, 2022, pp. 121–126. doi:10.1109/EMBC48229.2022.9871266.
- [54] S. Śmigiel, K. Pałczyński, D. Ledziński, Ecg signal classification using deep learning techniques based on the ptb-xl dataset, *Entropy* 23 (2021) 1121.
- [55] J. Wang, X. Qiao, C. Liu, X. Wang, Y. Liu, L. Yao, H. Zhang, Automated ecg classification using a non-local convolutional block attention module, *Computer Methods and Programs in Biomedicine* 203 (2021) 106006.

Supplementary File

Appendix A. Evaluation Metrics

We utilize common metrics in ML (precision (Eq. A.1), recall (Eq. A.2), and F1 score (Eq. A.3)), and present a set of custom evaluation metrics used to assess the plausibility of the generated counterfactual clues for ECG signals. The metrics are designed to capture both the clinical relevance of the counterfactual changes and the simplicity of the explanations.

In the custom evaluation, we initiated a blind evaluation by providing domain experts with raw ECG reports to establish a baseline and enrich our visual evaluation with additional data. Subsequently, we issued four primary instructions to the domain experts for validating the generated visual reports. In the first evaluation, we requested them to assess the report’s interpretability and quality as a cognitive task. In the second evaluation, we asked them to identify individual errors in selecting clues for the visualization and to evaluate the alignment with a blind evaluation. For the third evaluation, we requested them to rate the clinical relevance of our visualized clues on a scale from 0 to 5, which we considered as a visualization validity score. Finally, we asked them to assess the overall clinical significance of the selected features to determine the weighted sparsity of the counterfactuals. We have also made the labels assigned by clinicians for specific instructions available on our GitHub page <https://github.com/tanyelai/vcce>.

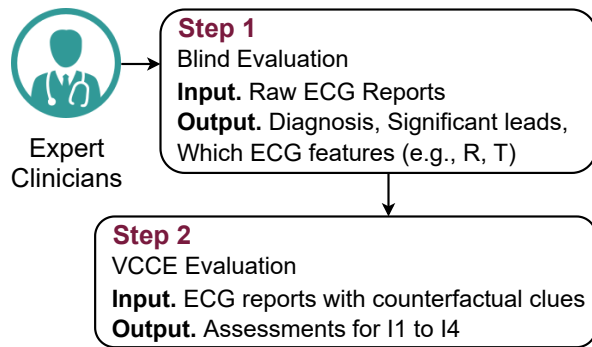


Figure Appendix A.1: Evaluation process of the domain experts.

Precision, Recall and F1 Score. We assessed the ML models using Precision, a measure of correct positive predictions; Recall, the model’s ability to identify all positives; and the F1 Score, a balance between Precision and Recall, especially useful in imbalanced datasets. In classification tasks, True Positives (TP) are instances

correctly predicted as positive, False Positives (FP) are instances incorrectly predicted as positive, and False Negatives (FN) are instances incorrectly predicted as negative. The validation metrics used in ML are as following equations:

$$\text{Precision} = \frac{\text{TP}}{\text{TP} + \text{FP}} \quad (\text{A.1})$$

$$\text{Recall} = \frac{\text{TP}}{\text{TP} + \text{FN}} \quad (\text{A.2})$$

$$\text{F1 Score} = 2 \times \frac{\text{Precision} \times \text{Recall}}{\text{Precision} + \text{Recall}} \quad (\text{A.3})$$

Directions to Measure Custom Metrics. The simplified instructions for cardiologists consist of two main parts: blind evaluation and visualized clues evaluation (Figure Appendix A.1). Each patient has two ECG reports: an original and a marked one. The original reports will be used to assess clinical consistency, while the marked reports will be used to evaluate cognitive aspects of the method, including its ‘understandability,’ ‘interpretability,’ and ‘plausibility.’

1. **Blind:** A diagnosis will be established based on the original ECG; this diagnosis will outline which leads are significant and which cardiac characteristics are being assessed clinically.
2. **Visualized Clues:** We test the clarity and accuracy of the marked areas with our method under the following four instructions (I):
 - I-1:** Can the meanings of the markings be understood? Evaluate their interpretability and quality as ‘low,’ ‘moderate,’ or ‘good’.
 - I-2:** Does it make sense for the mark to be here? Please also provide the total count of incorrect marks in the given report.
 - I-3:** Are the marked signal features clinically significant (if not marked, write "None")? If they are significant, please rate their importance between 1-5. If they are not significant but are marked, enter 0. If they are not significant and are also not marked (indicating the correct decision of non-selection), reward this accuracy by entering 5.
 - I-4:** In order to evaluate overall feature selection, please rate how clinically significant our chosen 24 features are for you on a scale of 0-24.

Clinical Interpretability Score (I-1). reflects the ease with which the clinicians can understand and interpret the counterfactual clues. This score is a qualitative assessment provided by the clinicians, indicating the level of interpretability (i.e., ‘low,’ ‘moderate,’ ‘good’).

Clinical Outcome Alignment Score (I-2). quantifies the extent to which the predicted clinical outcomes of the counterfactual explanations align with the experts’ assessments of potential clinical outcomes. Given the cardiologists’ list of important leads obtained through blind evaluation, we introduce a weight W_i for each lead, where $W_i = 3$ if the i^{th} lead is in the important lead list, and $W_i = 1$ otherwise. The alignment (A) score is then calculated using counterfactuals (cf) as follows:

$$A = \frac{\sum_{i=1}^n (W_i \cdot \text{Indicator}(\text{Lead } i \text{ aligned with cf}))}{\max(\sum_{i=1}^n W_i, 1)} \quad (\text{A.4})$$

Where:

- n is the total number of leads considered.
- W_i is the weight of the i^{th} lead, which is 3 if the lead is in the cardiologists’ important lead list, and 1 otherwise.
- The Indicator function returns 1 if the i^{th} lead is aligned with the counterfactuals, and 0 otherwise.

The denominator $\max(\sum_{i=1}^n W_i, 1)$ ensures that the alignment score is normalized to the interval $[0, 1]$, even in cases where the weight of important leads could potentially make the score greater than 1.

Visualization Validity Score (I-3). gauges the clinical relevance of generated visual clues displayed on the ECG. The Visualization Validity Score (VVS) for each patient is the summation of scores from individual visual clues, offering insight into the validity of the VCCE.

Given visual clues based on the P, Q, R, S, T waveforms, the VVS for each patient is formulated as:

$$\text{VVS} = \sum_{i=1}^5 \text{Score}_i \quad (\text{A.5})$$

where Score_i represents the score assigned to the i^{th} waveform by the clinician.

Feature Importance Weighted Sparsity Score (I-4). This metric is designed to measure both the influence and sparsity of each ECG feature when generating counterfactual explanations. By evaluating the interaction between the feature’s sparsity and its clinical or XGBoost-derived importance, it allows for more insightful and reliable interpretations.

Given m counterfactuals, n ECG features, and the respective weights w_{mi} (clinical or XGBoost) for the i^{th} feature, the sparsity scores $S_{\text{method},j}$ for the j^{th} counterfactual are computed using deviations x_{ij} from the original instance. The overall mean and standard deviation for each sparsity score method are denoted by \bar{S}_{method} and $\sigma_{S_{\text{method}}}$ respectively.

The sparsity scores based on the method can be represented as:

$$\bar{S}_{\text{method}} = \frac{1}{m} \sum_{j=1}^m \left(\sum_{i=1}^n |x_{ij} \cdot w_{mi}| \right), \quad (\text{A.6})$$

$$\sigma_{S_{\text{method}}} = \sqrt{\frac{1}{m} \sum_{j=1}^m \left(\sum_{i=1}^n |x_{ij} \cdot w_{mi}| - \bar{S}_{\text{method}} \right)^2} \quad (\text{A.7})$$

where $\text{method} \in \{\text{clinical, XGBoost}\}$ and w_{mi} is the weight corresponding to the chosen method.

A higher value of \bar{S} indicates the importance of specific ECG features in counterfactual explanations, while the associated σ quantifies variability across different instances.

Model Name	Accuracy	Precision	Recall	F1-Score	AUC-ROC
XGBoost*	89.44	89.74	87.99	88.73	89.36
AdaBoost	84.80	84.74	82.75	83.73	84.70
Gradient Boosting	87.74	88.49	85.12	86.78	87.60
Extra Trees	87.67 (0.08)	88.28 (0.22)	85.23 (0.13)	86.73 (0.06)	87.55 (0.07)
Random Forest	87.68 (0.07)	89.03 (0.13)	84.31 (0.27)	86.61 (0.10)	87.50 (0.08)
Logistic Regression	83.85	83.27	82.37	82.82	83.77
Support Vector Machine	87.96	88.55	85.58	87.04	87.83
Gaussian Naive Bayes	74.57	68.72	84.77	75.91	75.10
K-Nearest Neighbors	82.57	79.78	84.56	82.10	82.68

Table Appendix A.1: Machine learning models’ outcomes for the utilized dataset on different trials, with the standard deviation of randomly initialized trees shown in brackets. XGBoost* results denote statistically significant differences compared to other models (p-value < 0.01). We applied McNemar’s test, which is designed to assess whether there is a significant difference in the proportions of correct and incorrect predictions between the two models.

Appendix B. Model Selection

Table Appendix A.1 illustrates the comparative performance of several machine learning models applied to our dataset. Among the evaluated models, XGBoost emerged as the most proficient, achieving the highest scores across all metrics, including Accuracy (89.44%), Precision (89.74%), Recall (87.99%), F1-Score (88.73%), and AUC-ROC (89.36%). In contrast, the Gaussian Naive Bayes model exhibited the lowest accuracy and precision, yet it achieved a relatively high recall of 84.77%. The ensemble models such as Random Forest, Gradient Boosting, AdaBoost, and Extra Trees, along with the Support Vector Machine, demonstrated decent efficacy. Furthermore, Logistic Regression and K-Nearest Neighbors provided moderate reliability and scores. We opted for the XGBoost model in this study because it maintains a balance across all metrics and offers the highest scores.

Appendix C. Figures

We do not present numerical results for denoising and peak detection as they are out of scope; however, we conducted experimental assessments during method selection. We explored various techniques, and their efficacy varied across different random patients—some were beneficial while others were not. Certainly, we found no universally applicable method that effectively identified peaks in all the patients we studied. In patients with a substantial amount of noise, the selection of peaks can deviate, impacting the outcomes, and this deviation is inevitable for most patients, even with methods that are substantiated in the current literature.

The Figure Appendix C.2 illustrates the distribution of raw and denoised signals across various leads for a selected beat within the population. It is important to note that individual investigations might encounter significant noise, and this figure serves as an example to showcase the substantial variance in beats across the population. Moreover, the figure visibly demonstrates the considerable discrepancy in signal amplitude values between the NORM and MI populations.

The effect of denoising on one beat is demonstrated for two random samples in Figure Appendix C.3. Moreover, in Figure Appendix C.4, we can also observe how the signal in each lead changes discretely for the samples.

To make the durations more conspicuous, you can see the elapsed times for sample 50 beats with 5, 10, 15, 20 feature counts in Figure Appendix C.6a and Appendix C.6b.

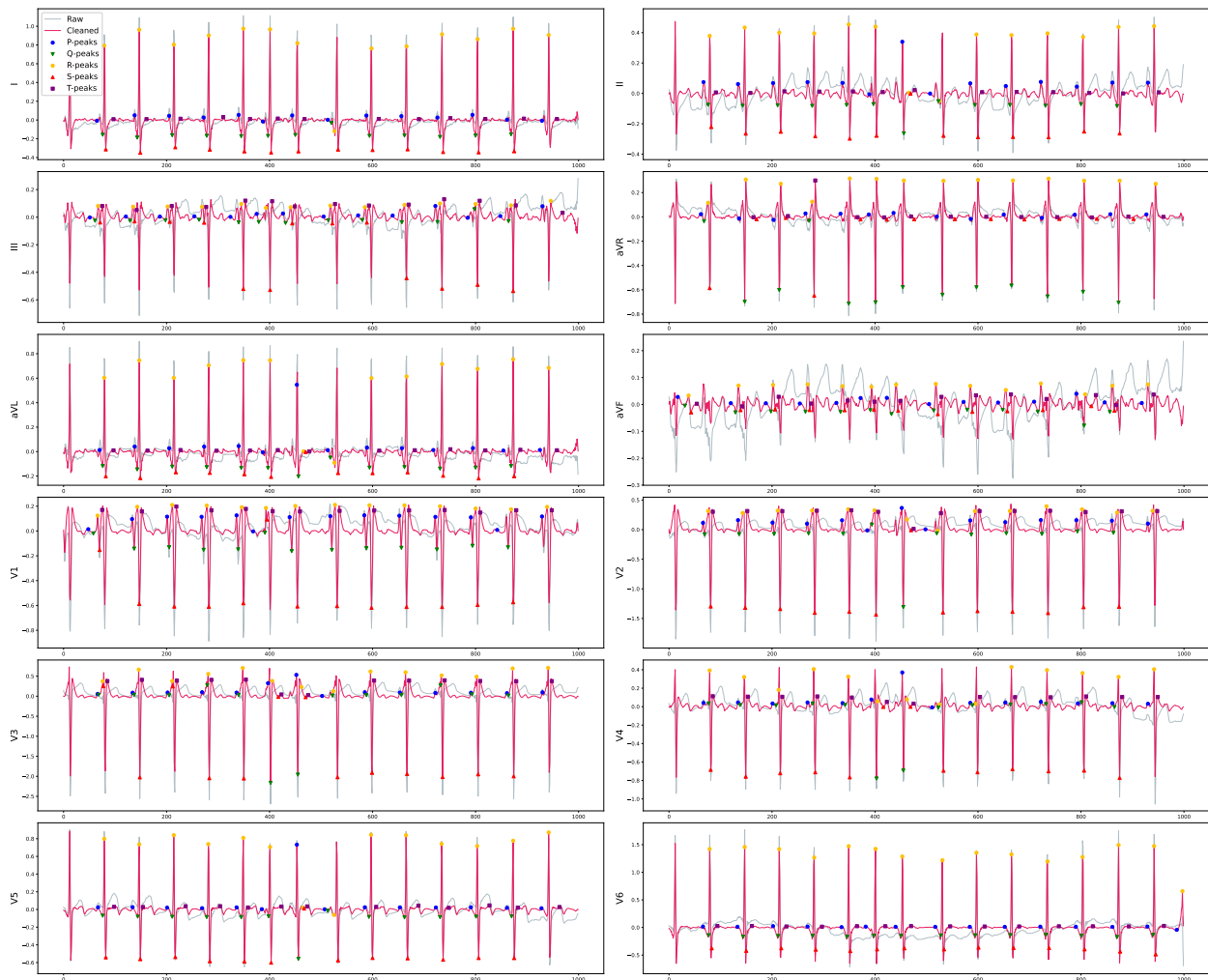


Figure Appendix C.1: Denoising and peaks detection using koka2022 method for a random MI patient.

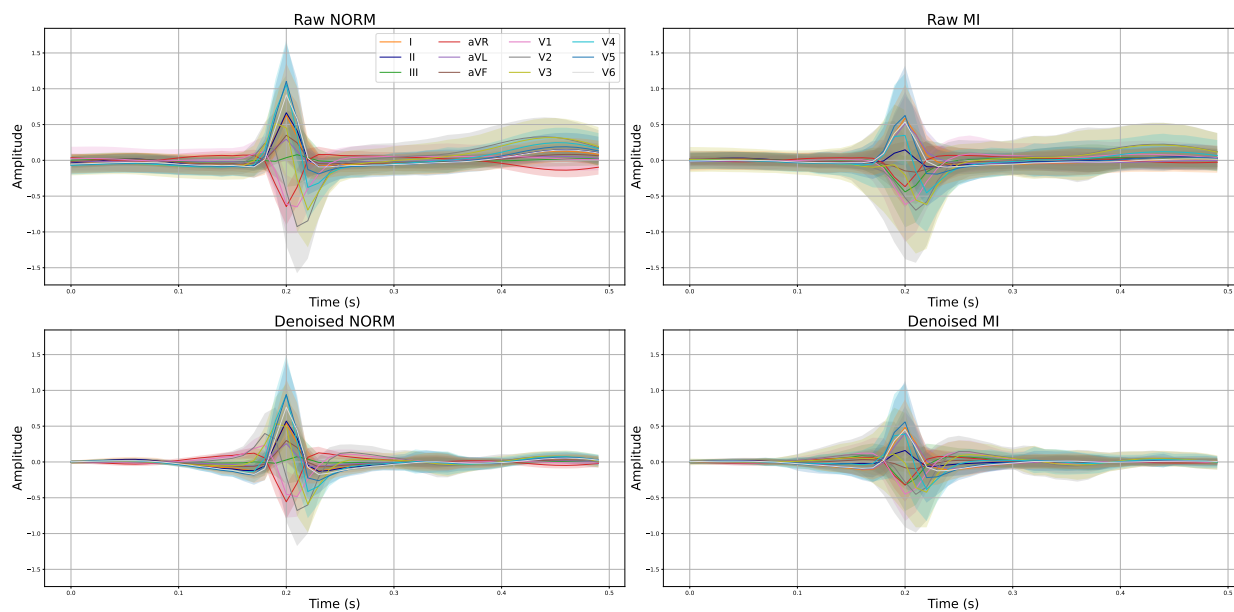


Figure Appendix C.2: The mean and standard deviation of 12-lead data are compared before and after preprocessing using the “koka2022” method at one beat. The lines serve as references for the population mean, while the emphases are on illustrating the standard deviation.

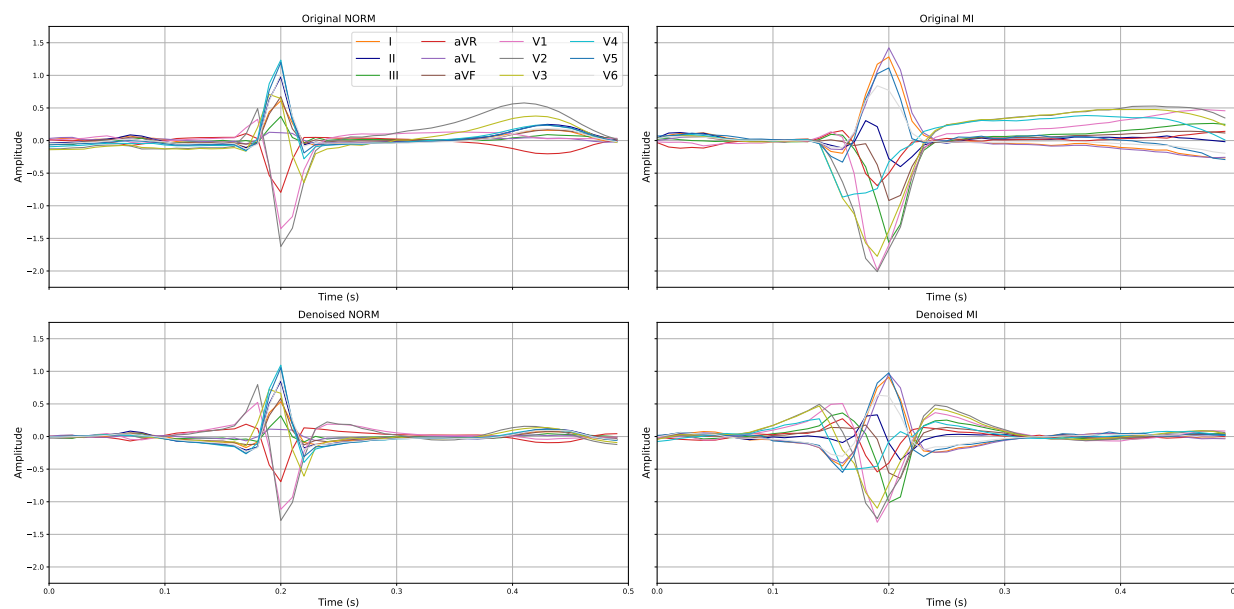


Figure Appendix C.3: Impact of denoising on one random NORM and MI patients on third beat.

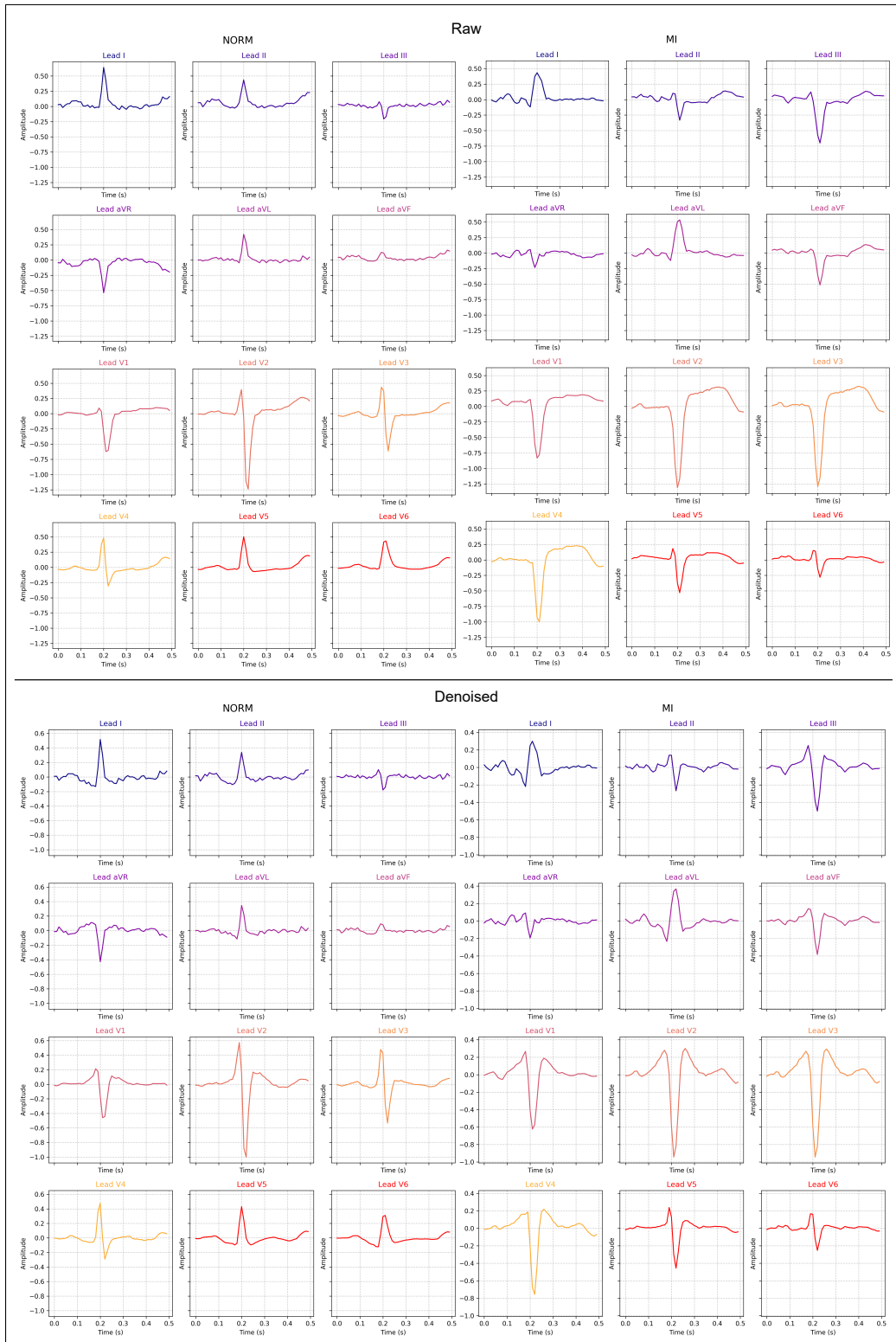
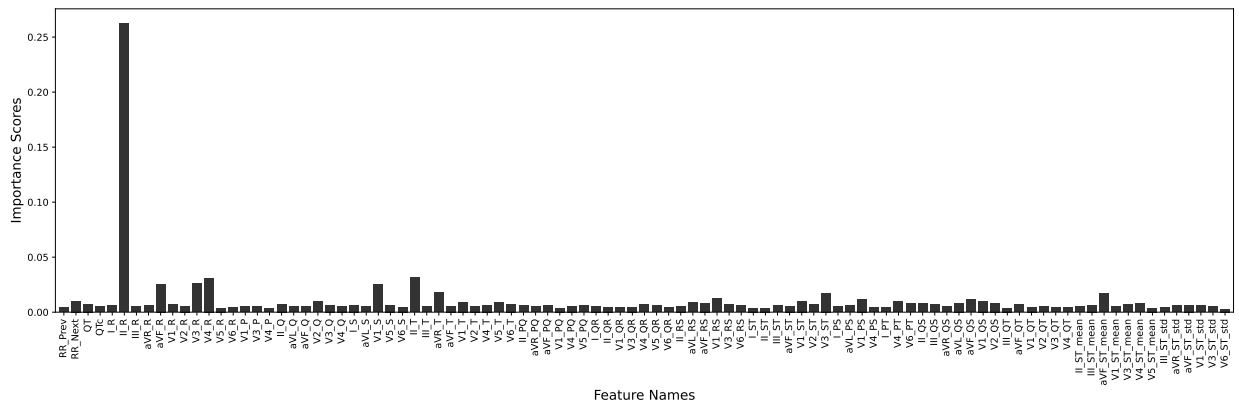
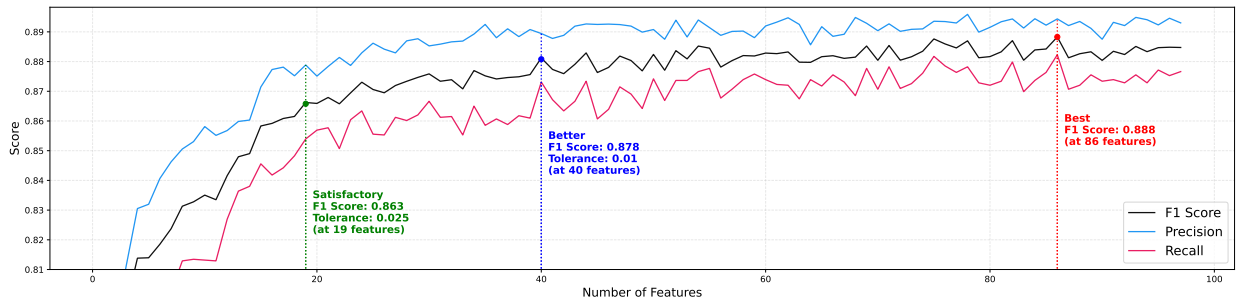


Figure Appendix C.4: Beat-level example before and after denoising for one random NORM and MI patients.

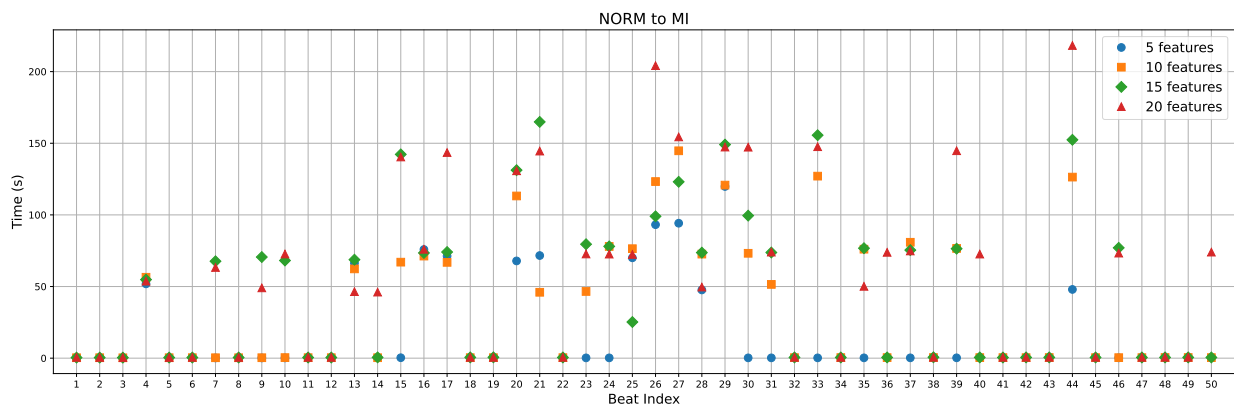


(a) The importance report for each chosen feature in the classification of NORM and MI.

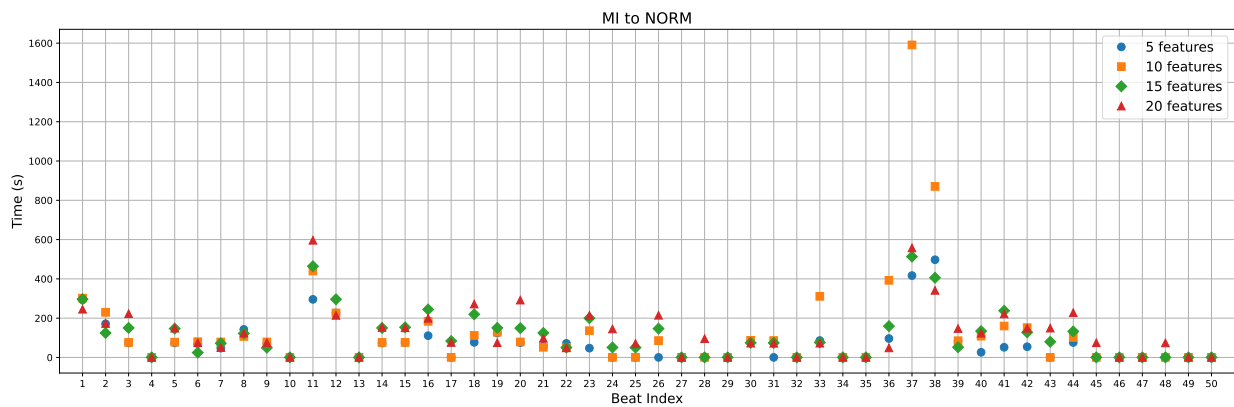


(b) Control subjects and myocardial infarction patients classification with ascending counts for selected features.

Figure Appendix C.5: Feature importance report and classification performance with selected features.



(a) Required time to generate counterfactuals for NORM to MI.



(b) Required time to generate counterfactuals for MI to NORM.

Figure Appendix C.6: Comparison of time required to generate counterfactuals between NORM and MI, and vice versa.



Figure Appendix C.8: Accurate Visualization (id: 1303.0): The specified ECG shows ST elevation in V1-V2-V3 derivations. The model correctly identified the loss of R progression in V3, deep S wave in V1, and ST-T changes in V1. In the PTB-XL dataset, this ECG was incorrectly evaluated as normal, our label is anterior MI.



Figure Appendix C.9: False Detection Due to VES (id: 16448): In the specified ECG, the presence of bigeminy ventricular ectopic beats (VES) led the model to primarily evaluate these beats rather than the sinus beats (D2, V2, V4). This resulted in incorrect labeling by our method.

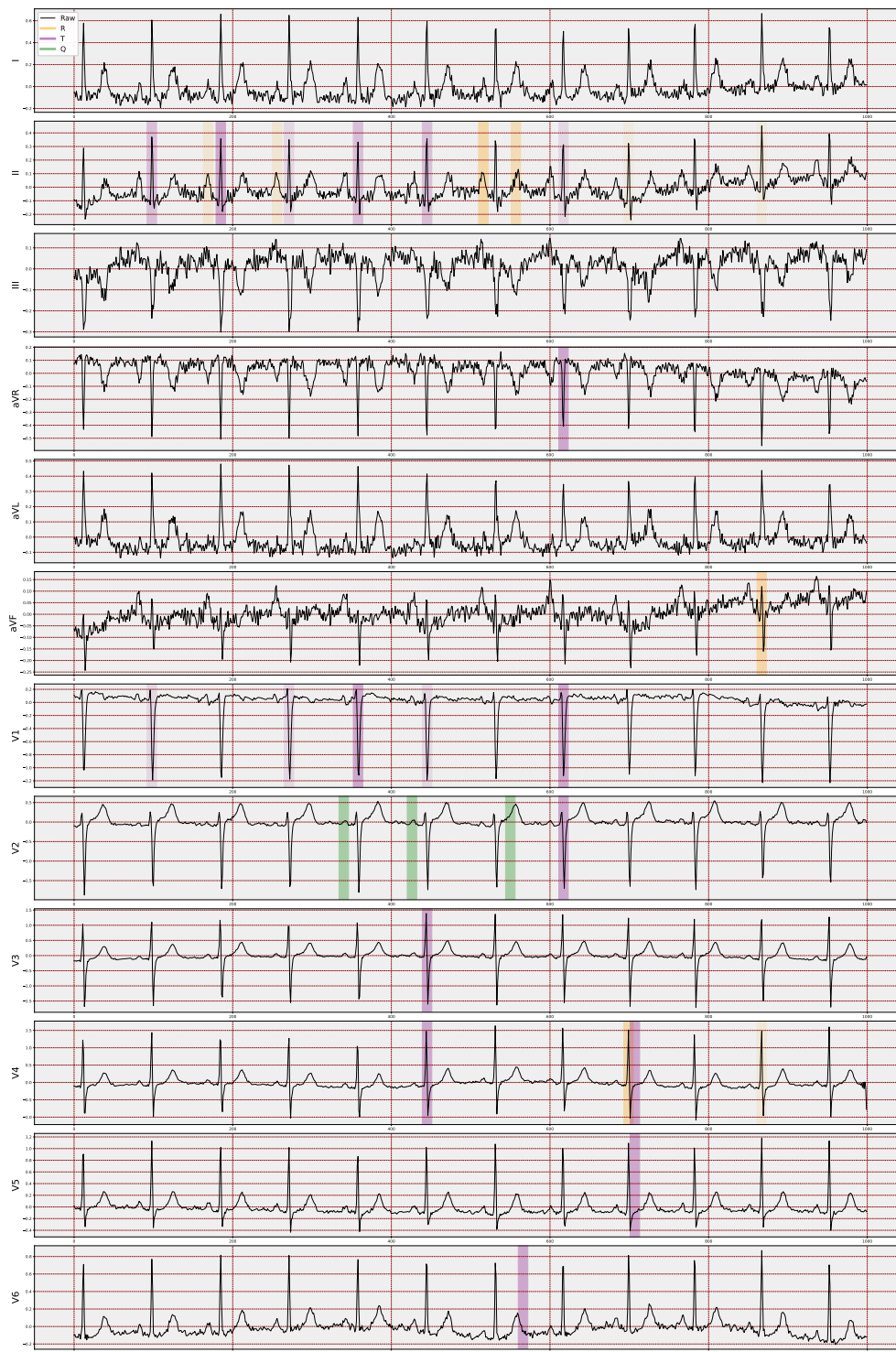


Figure Appendix C.10: False Detection Due to Artifact (id: 2261): In the specified ECG, artifacts observed, especially in the extremity derivations, could be attributed to possible muscle or neurological diseases. Consequently, our method exhibited a high error rate for this case, primarily due to the peak detection algorithm's inability to effectively manage the artifacts present in the signal. The PTB-XL dataset also contains instances where artifacts were mistakenly interpreted as potential inferior MIs, leading to incorrect diagnoses of inferior infarctions.